




RESEARCH ARTICLE

An improved wide-lane ambiguity resolution method for kinematic smartphone positioning

Yan Zhang,¹ Yang Jiang,^{1*}  Yuting Gao,² Shuai Guo,¹ and Yang Gao¹

¹Department of Geomatics Engineering, University of Calgary, Calgary, Canada

²College of Geomatics, Xi'an University of Science and Technology, Xi'an, China.

*Corresponding author: Yang Jiang; Email: yang.jiang1@ucalgary.ca

Received: 15 May 2023; **Revised:** 15 March 2024; **Accepted:** 24 April 2024

Keywords: smartphone precise positioning; wide-lane integer ambiguity resolution; partial ambiguity resolution (PAR); real-time kinematics (RTK); global navigation satellite system (GNSS)

Abstract

The release of GNSS raw data on Android smartphones provides the potential for high-precision smartphone positioning using multi-constellation and multi-frequency signals. However, severe multipath and low observation quality in kinematic environments make double-differenced uncombined ambiguities difficult to resolve reliably. To address this, the paper proposes an improved wide-lane (WL) integer ambiguity resolution (IAR) method that combines integer rounding and the Least-Square AMBIGUITY Decorrelation Adjustment (LAMBDA) methods. The proposed method achieved fix rates of 57% to 70% in challenging environments, with an average improvement of 7.7% in horizontal positioning accuracy compared to the float solution. The traditional partial integer rounding method only improved accuracy by 1.1%.

1. Introduction

In recent years, smartphone positioning and navigation services have become a hot research topic with many potential applications (Engelbrecht et al., 2015; Paziewski, 2020). In 2016, Google made the GNSS raw observation data accessible to Android 7.0 smartphone users so that precise positioning became feasible with new-generation smartphones (European GSA, 2018a). Since then, many progresses have been made including support of multi-constellation and multi-frequency signal tracking with smartphone GNSS modules. For instance, the Mi 8 released in 2018 from Xiaomi is equipped with the Broadcom BCM47755 chipset supporting L1 + L5 dual-frequency GNSS signals (European GSA, 2018b). The Google Pixel 4 is embedded with the Qualcomm Snapdragon 855 chipset and supports L1 + L5, E1 + E5a, and B1 signals. With navigation signals from multiple constellations and multiple frequencies, ambiguity resolution (AR) with smartphone GNSS measurements becomes feasible for precise positioning.

Several attempts have been made on resolving double-differenced L1 or L5 ambiguities, such as in Gao et al. (2021), Li and Geng (2022), Li et al. (2022a) and Yong et al. (2022). However, the trials were conducted based on data acquired in open sky environments, so they cannot be applied to applications in environments with severe multipath and low observation quality. Compared to methods that directly fix the L1 and L5 ambiguities, wide-lane (WL) integer ambiguity resolution (IAR) is more realistic in this case, since it has relatively longer wavelengths to correctly find the integer cycles, especially when encountering limited measurement quality and redundancy (Geng et al., 2011). In WL IAR, Hatch-Melbourne-Wübbena WL (HMW-WL) linear combination (Hatch, 1983; Melbourne, 1985;

Wübbena, 1985) is widely utilized, where the effects of the atmosphere delay and the clocks are eliminated. Geng and Bock (2013) proposed a WL IAR method based on a geometry-based ionosphere-free (IF) combination for triple-frequency observations. Gu et al. (2015) used BDS-2 observations of a small network to fix the extra-wide-lane and WL ambiguities. Those investigations show that WL IAR can improve the positioning performance with low-cost GNSS modules used in smartphones. To date, few attempts have been made to achieve WL IAR or AR on L1 and L5 in kinematic environments. This is because the pseudorange measurements will experience large and unstable noise variations that will decrease the success rate of AR. The studies based on double-differenced smartphone positioning without AR, called a float solution, can be found in Realini et al. (2017) and Dabove and Di Pietra (2019a), where meter-level accuracy can be obtainable under kinematic conditions. To improve the performance, stochastic modelling methods for smartphone GNSS positioning have been investigated, for example in Dabove and Di Pietra (2019b) and Li et al. (2022b). Since smartphone GNSS measurements can contain faulty pseudorange and carrier-phase measurements which lead to large positioning errors in kinematic environments, robust estimation methods such as factor graph optimization have been proposed (Suzuki, 2021, 2022; Jiang et al., 2022). Currently, the achievable positioning accuracy in kinematic environments is at the 1-meter-level. Although WL IAR has the potential to improve positioning accuracy in kinematic environments, the carrier-phase measurements suffer from ambiguity biases, such as initial phase bias (IPB), carrier-phase multipath and antenna offset (Geng and Li, 2019), which means only partial fixing is feasible on smartphones (Wen et al., 2020; Zeng et al., 2022). Until recently, WL ambiguities on smartphones have drawn attention (Gao et al., 2023; Hu et al., 2023), where a reliable and accuracy smartphone WL IAR solution is still denied.

In this study, we propose an improved WL IAR method to enhance smartphone precise positioning, which takes the existence of ambiguity biases into account and develops ways to minimize their effect. The proposed method consists of several steps. In the first step, the float ambiguities with significant confidence function values are processed with integer rounding (Teunissen, 2001). These ambiguities are constrained to increase the accuracy of the rest ambiguities, where the computational load is also greatly reduced compared with the traditional method. In the second step, the remainder of the float ambiguities are handled by the Least-Square AMBIGUITY Decorrelation Adjustment (LAMBDA) (Teunissen, 1993, 2001) method. By transforming the ambiguity estimates to a new set where the estimates are less correlated with each other, the LAMBDA method significantly reduces the searching space for ambiguity resolution. Due to the poor quality of smartphone GNSS data and insufficient number of phase observations as well as numerical computation accuracy limitation, the covariance matrix of the float ambiguities can become non-positive definite after the least-squares estimation (Dong et al., 2022; Song et al., 2022). This will lead to the failure of LD factorization during the LAMBDA process for searching integer ambiguities. A procedure of matrix reconstruction has been proposed to overcome the non-positive definite problem, where the float ambiguities are divided into groups and are fixed sequentially to reduce the computational load. To evaluate the property of smartphone WL ambiguities and WL IAR efficiency with smartphone GNSS observations using the proposed method, the datasets from different smartphones in kinematic environments from GSDC are applied.

The rest of this paper is arranged as follows. The mathematical models of WL IAR, the matrix reconstruction and the grouped ambiguity are described in the second section. The data used in our experiment are described in the third section. The smartphone positioning performance with the proposed WL IAR method and the evaluation of different smartphones are also introduced. Finally, the findings and conclusions are summarized in the last section.

2. Methodology

This section explains in detail the methodology used in this study. First, the method to produce the float ambiguity resolutions for smartphone devices is discussed. Second, the proposed WL IAR method is presented.

2.1. Float-ambiguity solution based on least-squares

Real-time kinematic (RTK) technology is a commonly used technology in GNSS high-precision positioning to obtain high accuracy in a short period of time and meet the needs of smartphone positioning services. To investigate the WL IAR estimation in smartphone positioning with RTK, we start it from the dual-frequency observation equation for pseudorange and carrier phase:

$$\begin{cases} P_{r,f}^s = \rho_r^s + cdt_r - cdt^s + m_h T_r^s + I_r^s + b_{r,f} - b_f^s + \tau_{bias_{r,f}} + m_f + \epsilon_f \\ L_{r,f}^s = \lambda_f \varphi_{r,f}^s = \rho_r^s + cdt_r - cdt^s + m_h T_r^s + I_r^s + \lambda_f N_f + \lambda_f d_{r,f} - \lambda_f d_f^s + \kappa_{bias_{r,f}} + m_f + \epsilon_f \end{cases} \quad (1)$$

where $P_{r,f}^s$ and $L_{r,f}^s$ are pseudorange and carrier phase ranges at frequency $f (f = 1, 2)$; r and s represent receiver and satellite; $\varphi_{r,f}^s$ is the raw phases; ρ_r^s is the geometric distance; dt_r and dt^s denote the clock offset of receiver and satellite; c is the speed of light in vacuum; T_r^s is the zenith tropospheric delay; m_h is the mapping function; I_r^s is the ionospheric delay; $b_{r,f}$ and b_f^s are receiver-dependent and satellite-dependent hardware delay of pseudorange observables at frequency f ; $d_{r,f}$ and d_f^s are the receiver-dependent and satellite-dependent hardware delay of phase observables at frequency f ; $\tau_{bias_{r,f}}$ and $\kappa_{bias_{r,f}}$ are the receiver-related code bias and phase bias at frequency f ; N_f is the single-differenced ambiguity for satellite s relative to a reference satellite at frequency f ; λ_f is the wavelength of f frequency; and m_f and ϵ_f are multipath effect and observational noise.

According to (1), the double-difference (DD) between two receivers (r, b) and two satellites (i, j) can be expressed as:

$$\begin{cases} \Delta \nabla P_{rb,f}^{ij} = \Delta \nabla \rho_{rb,f}^{ij} + \Delta \nabla I_{rb,f}^{ij} + m_h \Delta \nabla T_{rb,f}^{ij} + \Delta \nabla \epsilon_{P_{rb,f}^{ij}} \\ \lambda_f \Delta \nabla \varphi_{rb,f}^{ij} = \Delta \nabla \rho_{rb,f}^{ij} - \Delta \nabla I_{rb,f}^{ij} + m_h \Delta \nabla T_{rb,f}^{ij} + \lambda_f (N_{rb,f}^i - N_{rb,f}^j) + \Delta \nabla \epsilon_{\varphi_{rb,f}^{ij}} \end{cases} \quad (2)$$

where r and b indicate rover and base receiver; $\Delta \nabla$ is the DD operator; $\Delta \nabla P_{rb,f}^{ij}$ and $\Delta \nabla \varphi_{rb,f}^{ij}$ are the DD pseudorange and phase observables at frequency f ; $\Delta \nabla I_{rb,f}^{ij}$ is the DD ionospheric delay; $\Delta \nabla T_{rb,f}^{ij}$ is the DD zenith tropospheric delay; and $\Delta \nabla \epsilon_{P_{rb,f}^{ij}}$ and $\Delta \nabla \epsilon_{\varphi_{rb,f}^{ij}}$ are the DD observational noise and multipath error.

Due to the short baselines of GSDC datasets, the residuals of ionospheric delay can be built by the broadcast model, and the wet tropospheric delay can be modelled with the constant. Therefore, the matrix form of DD with m satellites in one epoch can be figured out:

$$\begin{aligned} Z &= HX + v R \quad (3) \\ Z_{4m \times 1} &= \begin{bmatrix} \Delta \nabla P_{rb,f}^{i1} - \Delta \nabla \rho_{rb,f}^{i1} - \Delta \nabla I_{rb,f}^{i1} - m_h \Delta \nabla T_{rb,f}^{i1} - \Delta \nabla \epsilon_{P_{rb,f}^{i1}} \\ \lambda_f \Delta \nabla \varphi_{rb,f}^{i1} - \Delta \nabla \rho_{rb,f}^{i1} + \Delta \nabla I_{rb,f}^{i1} - m_h \Delta \nabla T_{rb,f}^{i1} - \lambda_f (N_{rb,f}^i - N_{rb,f}^1) - \Delta \nabla \epsilon_{\varphi_{rb,f}^{i1}} \\ \vdots \\ \Delta \nabla P_{rb,f}^{im} - \Delta \nabla \rho_{rb,f}^{im} - \Delta \nabla I_{rb,f}^{im} - m_h \Delta \nabla T_{rb,f}^{im} - \Delta \nabla \epsilon_{P_{rb,f}^{im}} \\ \lambda_f \Delta \nabla \varphi_{rb,f}^{im} - \Delta \nabla \rho_{rb,f}^{im} + \Delta \nabla I_{rb,f}^{im} - m_h \Delta \nabla T_{rb,f}^{im} - \lambda_f (N_{rb,f}^i - N_{rb,f}^m) - \Delta \nabla \epsilon_{\varphi_{rb,f}^{im}} \end{bmatrix} \quad (4) \end{aligned}$$

$$H_{4m \times 5} = \begin{bmatrix} \frac{{}^1\partial\rho_{rb,f}^{i1}}{\partial x} & \frac{{}^1\partial\rho_{rb,f}^{i1}}{\partial y} & \frac{{}^1\partial\rho_{rb,f}^{i1}}{\partial z} & 0 & 0 \\ \frac{{}^1\partial\rho_{rb,f}^{i1}}{\partial x} & \frac{{}^1\partial\rho_{rb,f}^{i1}}{\partial y} & \frac{{}^1\partial\rho_{rb,f}^{i1}}{\partial z} & \lambda_f & -\lambda_f \\ \vdots & \vdots & \vdots & \vdots & \vdots \\ \frac{{}^m\partial\rho_{rb,f}^{im}}{\partial x} & \frac{{}^m\partial\rho_{rb,f}^{im}}{\partial y} & \frac{{}^m\partial\rho_{rb,f}^{im}}{\partial z} & 0 & 0 \\ \frac{{}^m\partial\rho_{rb,f}^{im}}{\partial x} & \frac{{}^m\partial\rho_{rb,f}^{im}}{\partial y} & \frac{{}^m\partial\rho_{rb,f}^{im}}{\partial z} & \lambda_f & -\lambda_f \end{bmatrix} X_{5 \times 1} = \begin{bmatrix} x \\ y \\ z \\ N_{rb,f}^i \\ N_{rb,f}^j \end{bmatrix} R_{4m \times 4m} \quad (5)$$

where Z , H and R represent the DD observation matrix, the DD design matrix and the DD variance-covariance matrix of while noise v . After combining all the epochs of GNSS observations, we use the least-square method to estimate the coordinates and the float WL ambiguities. Here, satellite i is defined as reference satellite, the reference satellite ambiguity $N_{rb,f}^i$ is set to arbitrary integer value, thus the dual-frequency WL ambiguity can be calculated as:

$$N_{rb,f}^{ij} = (N_{rb,1}^i - N_{rb,2}^i) - (N_{rb,1}^j - N_{rb,2}^j) \quad (6)$$

Based on a least-squares estimation scheme, the float WL ambiguities can be derived:

$$B_{WL} = D * \hat{X} \quad (7)$$

$$D_\alpha = [0 \ 0 \ 0 \ 1 \ -1 \ \dots \ -1 \ 1] \quad (8)$$

$$D = [D_1 \ D_2 \ \dots \ D_\alpha] \quad (9)$$

$$\hat{X} = [x \ y \ z \ N_{rb,1}^i \ N_{rb,2}^i \ N_{rb,1}^j \ N_{rb,2}^j \ \dots \ N_{rb,1}^m \ N_{rb,2}^m]^T \quad (10)$$

where the \hat{X} is the full solution of DD; $[1 \ -1 \ \dots \ -1 \ 1]$ stands for $[N_{rb,1}^i \ -N_{rb,2}^i \ \dots \ -N_{rb,1}^j \ N_{rb,2}^j]$. The variance-covariance matrix can be obtained:

$$Q_{WL} = D * P * D^T \quad (11)$$

$$P = \sigma_0^2 (H^T R^{-1} H)^{-1} \quad (12)$$

$$\sigma_0^2 = \frac{V^T R^{-1} V}{\gamma} \quad (13)$$

$$V = H\hat{X} - Z \quad (14)$$

Thus, the float ambiguities from these equations can be achieved. In the following part, we derive the proposed WL IAR method.

2.2. Proposed wide-lane ambiguity resolution method

Before the LAMBDA is applied, we first use the rounding method to directly fix the ambiguities within a certain threshold:

$$N_{WL,round} = (\text{round}(B_{WL}))_{\text{threshold}} \quad (15)$$

The remaining ambiguities is fixed by the LAMBDA algorithm. As the poor quality and frequent outliers in smartphone data, Q_{WL} matrix is not positive definite, this will lead us to be unable to perform LD factorization when using the LAMBDA method. To solve this problem, we apply the matrix

reconstruction method to keep Q_{WL} as positive definite (Brommer et al., 2020; Dong et al., 2022). First, Q_{WL} is decomposed with the form of eigenvector and eigenvalues:

$$Q_{WL} = V * Val * V^T \tag{16}$$

where V is the eigenvector of Q_{WL} ; $Val = \text{diag}(\text{val}_1, \text{val}_2 \dots)$, val_i is the eigenvalue of Q_{WL} . The negative of val_i is modified to positive by multiply -1, and the Q_{WL} is transformed to Q_{WL}^*

$$Q_{WL}^* = V * Val^* * V^T \tag{17}$$

Q_{WL}^* will become positive definite after iteration. Another issue must be considered is the amount of float WL ambiguities, lambda is hard to search results or wastes too much computational cost. One effective method is to build the float WL ambiguities groups by the adjacent epochs, the remaining ambiguities and variance covariance matrix can be expressed:

$$B_{WL, \text{lambda}} = \left[B_{WL,1}^1 \cdots B_{WL,m}^1 B_{WL,m+1}^2 \cdots B_{WL,2m}^2 B_{WL,m(p-1)+1}^p \cdots B_{WL,n}^p \right]^T \tag{18}$$

$$Q_{WL}^* = \begin{bmatrix} Q_{WL,k}^* & Q_{WL,k,p-k}^* \\ Q_{WL,p-k,k}^* & Q_{WL,p-k}^* \end{bmatrix} \quad k \in [1, p] \tag{19}$$

where m stands for the number of ambiguities for one group; p is the number of groups; n is the total number of ambiguities. The LAMBDA searching strategy is utilized with group-by-group, $B_{WL, \text{lambda}}$ and Q_{WL}^* must be updated accordingly after each set of ambiguity is fixed:

$$N_{WL,n-km}^* = B_{WL,n-km} - Q_{WL,p-k,k}^* (Q_{WL,p-k}^*)^{-1} * ({}^0 B_{WL,m}^k - B_{WL,m}^k) \tag{20}$$

$$Q_{WL,p-k}^* = Q_{WL,p-k}^* - Q_{WL,p-k,k}^* Q_{WL,k}^* (Q_{WL,p-k,k}^*)^T \tag{21}$$

where ${}^0 B_{WL,m}^k$ is the fixed WL ambiguities.

Figure 1 demonstrates the algorithm strategy of the WL IAR. The float ambiguities and the corresponding variance-covariance matrix are from sequential least-square method based on GNSS observations and broadcast ephemeris. The ambiguities-fixed strategy includes two steps, rounding and LAMBDA. The float ambiguities within a certain threshold of confidence function will be firstly fixed using the rounding method, then we filter out the remaining float ambiguities within another determined threshold. The variance-covariance matrix must be guaranteed to be positive definite before LAMBDA. After that, LAMBDA is launched with grouped float ambiguities and the corresponding variance-covariance matrix, and the two input factors are updated after each group is ambiguities-fixed. The confidence function is applied to determine the fixable ambiguities in rounding and LAMBDA methods according to the probability of the fix to the nearest integer, which can be described as (Dong and Bock, 1989; Ge et al., 2008):

$$\mu_0 = 1 - \sum_{\tau=1}^{\infty} \left[\text{erfc} \left(\frac{\tau - |b - n|}{\sqrt{2}\sigma} \right) - \text{erfc} \left(\frac{\tau + |b - n|}{\sqrt{2}\sigma} \right) \right] \tag{22}$$

and

$$\text{erfc}(x) = \frac{2}{\sqrt{\pi}} \int_x^{\infty} e^{-t^2} dt \tag{23}$$

where μ_0 is the possibility; b is the estimate ambiguity and σ is its STD; n is the nearest integer of b . The confidence function thresholds in our proposed method are flexible for users where the first one used by rounding method is 0.01%, and the second one for LAMBDA is 8%.

The following section discusses the experiment dataset to evaluate the performance of the proposed method, followed by the detailed result evaluations.

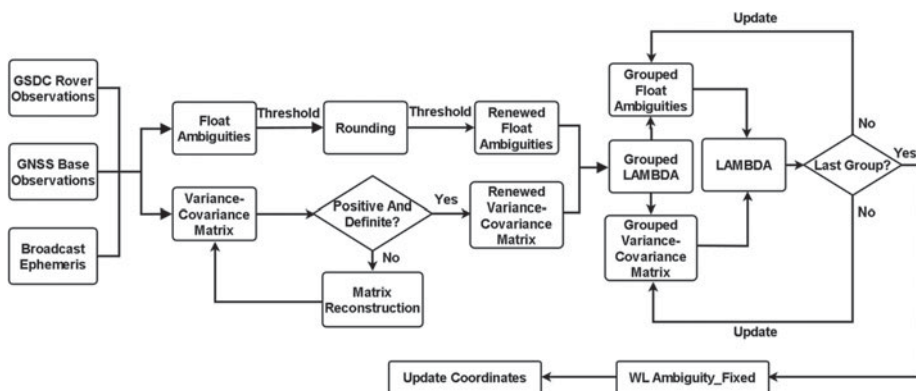


Figure 1. Flowchart of the proposed WL IAR method.

3. Experiment dataset from Google smartphone decimeter challenge 2022

To evaluate the proposed WL ambiguity resolution method for Android smartphones, this study uses the dataset of GSDC 2022, which is publicly available. Google held the GSDC in 2021 and 2022, who provided several datasets collected from different smartphones in kinematic real environments (Fu et al., 2020, 2022). Since the smartphones were placed inside vehicles that went through various types of environments, such as suburban, highway and dense urban, the processing of the Google datasets was a challenging task due to its low quality of pseudorange measurements and frequent carrier phase reset (Castel et al., 2021; Fortunato et al., 2021; Han et al., 2021; Kanhere et al., 2021; Dai, 2022). As reference, a NovAtel SPAN system is used during data collection with lever-arm calibration, which is mostly centimeter-level accurate. Figure 2 presents the environment of each trajectory in detail. As can be seen, the selected six trajectories have mostly covered highway and suburban environments, where their dataset IDs are 2020-12-10-US-SJC-2, 2020-05-29-US-MTV-1, 2020-08-13-US-MTV-1, 2021-01-05-US-MTV-2, 2021-07-19-US-MTV-1, 2021-12-08-US-LAX-5. In addition, their total time lengths are roughly 23.4, 31.3, 19.4, 31.6, 15.4, and 30.4 min, respectively. In those datasets, six different models of smartphones were involved, including the Google Pixel 4 (GP4), Google Pixel 4XL (GP4X), Google Pixel 5 (GP5), Google Pixel 6 Pro (GP6P), Xiaomi Mi 8 (XM8) and Samsung Galaxy S20 Ultra (S20 U). Accompanying the datasets, we also give the number of satellites and position dilution of precision (PDOP) of the six experimental trajectories. In Figure 3, the average of visible satellites for the used trajectories are 20.1, 21.2, 20.4, 18.5, 19.8 and 12.4. PDOP has a 97% probability of being between 0.8 and 1.5.

To process these datasets to obtain float solutions, the configurations in Table 1 are used. As an RTK processing scheme, we used the base station data provided by the UNAVCO organization; their information is summarized in Table 2. Overall, the receivers and antennas are survey-grade, with an average distance to the rover of 6.49 km.

In the following contents, three sections are presented to discuss the outcomes of the proposed method, including the property of smartphone WL ambiguities, positioning performances with WL IAR and a comparison of WL IAR between different smartphone models.

3.1. Property of smartphone wide-lane ambiguities

This section discusses the property of smartphone WL ambiguities. For the selected GSDC dataset in Section 3, the float solutions are obtained based on the method shown in Figure 1. We specifically assess the properties of smartphone WL ambiguities under such real environments in terms of four aspects: observability, uncertainty, integerness, and fix-rate. First, their observability is defined as the total number of epochs where a WL ambiguity is observed. Since RTK-based WL ambiguities correspond

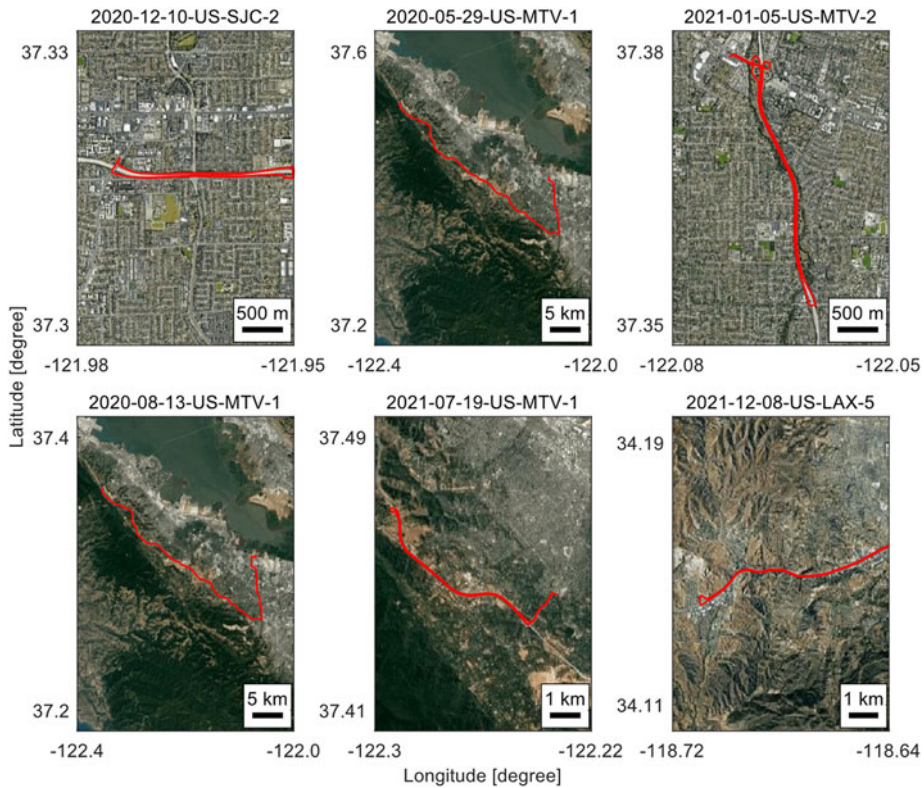


Figure 2. Environments for each trajectory from GSDC 2022 used in our experiment.

to linear combination of double-differenced dual-frequency measurements, the carrier-phases of both frequencies and satellites must be present to count for its observability. Second, to represent the success rate of WL IAR, their uncertainty can be described as their posterior variance after achieving the float solution, which is derived from Equation (12). Third, the closeness to integers of the float estimated WL ambiguities, which defines WL integerness, can also be obtained to roughly evaluate the quality of the float estimated smartphone WL ambiguities. Fourth, we show the proportions of the fixed WL ambiguities to the total numbers of WL ambiguities, defined as fix-rate in the sequel.

Figure 4 presents in detail the WL ambiguity observabilities of different smartphones on different trajectories in our experiment. The number of WL ambiguities enumerates all the WL ambiguities appearing in the float solutions. The average observability for smartphone-based WL ambiguities is $3 \cdot 36$ epochs, with a standard deviation of $6 \cdot 50$ epochs, where the average number of apparent WL ambiguities are $0 \cdot 99$ per epoch in our experiment. In all trajectories, 2020-08-13-US-MTV-1 and 2020-12-10-US-SJC-2 have the best and worst observabilities, which are $4 \cdot 94$ and $2 \cdot 70$ epochs for all WL ambiguities on average, respectively. For different smartphones, average WL observabilities are $4 \cdot 20$, $3 \cdot 83$, $3 \cdot 97$, $0 \cdot 79$, $4 \cdot 55$ and $1 \cdot 78$ epochs for GP4, GP4X, GP5, GP6P, XM8, and S20 U, respectively. As an initial conclusion, although smartphone devices do not have the observation quality equivalent to navigational GNSS devices, their WL ambiguities have the required observabilities for WL IAR.

Figure 5 shows the standard deviations of the estimated WL ambiguities from the float solution estimations, which represents the uncertainty of the WL ambiguities. Here, WL ambiguities from different trajectories are put together for different smartphones, which are 4, 2, 3, 1, 3 and 2 trajectories for GP4, GP4X, GP5, GP6P, XM8 and S20, respectively. Briefly, with a higher number of observabilities, generally reduced standard deviations can be reached. Specifically, the average standard deviation with observabilities from 1 to 10 epochs is $0 \cdot 153$, which is $0 \cdot 112$ with those from 11 to 20 epochs.

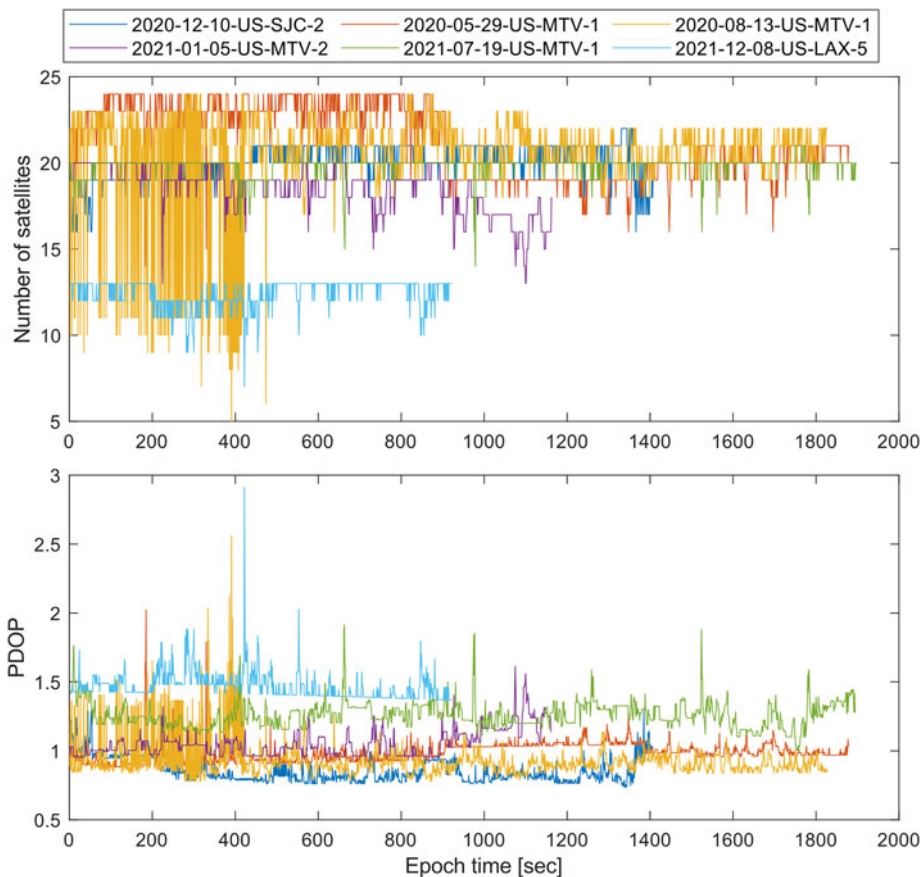


Figure 3. Number of satellites and PDOP for each trajectory from GSDC 2022 used in our experiment.

Table 1. Process configurations for float solutions.

Elevation angle cut-off	10.0°
Signal-to-noise ratio cut-off	20.0 dB – Hz
GNSS mode	RTK
Observation types used	Code-phase
System use	GPS + GLONASS + GALILEO
Base station	Provided by UNAVCO
Signals	GPS: L1 C/A + L5C; Galileo: E1 + E5a; GLONASS: L1 C/A
Minimum phase occurrences	5
Estimator	Global estimation based on least-squares
Measurement noise model	Elevation model
Ambiguity process noise	0.05 cycles
Coordinate process noise	30.0 m

Furthermore, assuming a three-timed standard deviation should be less than 1 cycle to safely execute WL IAR (which means standard deviation is less than $\frac{1}{3}$ cycles), the percentages of those WL ambiguities are 99.1%, 93.0%, 96.9%, 23.5%, 87.8% and 97.5% for GP4, GP4X, GP5, GP6P, XM8 and S20U, respectively. On average, the required observability should be 14,614 epochs. Here, GP6P does not have enough points, due its lack of data. As a conclusion, although the uncertainty of smartphone WL

Table 2. Base station data information in our experiment.

Trajectory name	Rovers	Base station ID	Average distance to the rover [km]	Receiver model	Antenna model
2020-12-10-US-SJC-2	GP4 GP4X GP5 XM8	P176	10·01	TRIMBLE NETR9	TRM59800.80
2020-05-29-US-MTV-1	GP4 GP4X	SLAC	1·96	TRIMBLE NETR9	TRM59800.80
2020-08-13-US-MTV-1	GP5	SLAC	3·51	TRIMBLE NETR9	TRM59800.80
2021-01-05-US-MTV-2	GP4 XM8	SLAC	13·60	TRIMBLE NETR9	TRM59800.80
2021-07-19-US-MTV-1	GP4 GP5 XM8 S20U	SLAC	6·55	TRIMBLE NETR9	TRM59800.80
2021-12-08-US-LAX-5	GP5 GP6P S20U	CBHS	3·30	SEPT POLARX5	ASH701945B_M

To simplify, the different rovers in trajectory 2020-12-10-US-SJC-2 are described by GP4 (Test 1), GP4X (Test 2), GP5 (Test 3) and XM8 (Test 4). Similar to this, the description in 2020-05-29-US-MTV-1 are GP4 (Test 5) and GP4X (Test 6); the description in 2020-08-13-US-MTV-1 is GP5 (Test 7); the description in 2021-01-05-US-MTV-2 are GP4 (Test 8) and XM8 (Test 9); the description in 2021-07-19-US-MTV-1 are GP4 (Test 10), GP5 (Test 11), XM8 (Test 12) and S20 U (Test 13); the description in 2021-12-08-US-LAX-5 are GP5 (Test 14), GP6P (Test 15) and S20 U (Test 16).

ambiguity is not acceptable for full WL IAR with 100% WL ambiguities, it has the potential to partially fix the WL ambiguities and increase the positioning performance.

Furthermore, Figure 6 displays the integerness of the estimated WL ambiguities, where all WL ambiguities from six trajectories and six smartphones are combined. Here, the integerness is represented by the integer residual value of $B_{WL} - \text{round}(B_{WL})$ in cycles. As can be seen, for the majority group of observability < 10 , the residual value is evenly distributed from -0.5 cycles to 0.5 cycles, which means they are not close to their correct integer values at all. The numbers of WL ambiguities in different ranges are 16,275, 330, 1,448 and 104 with observability < 10 , $10 \leq \text{observability} < 25$, $25 \leq \text{observability} < 50$, observability ≥ 50 , respectively. In this case, the integer rounding method is not likely to provide correct WL IAR solutions, and a decorrelation-involved method such as LAMBDA should be considered. For the WL ambiguities with better observability, the distribution remains similar, even when exceeding 25 epochs. This tells us some WL ambiguities are not actually fixable to integers, and therefore a partial WL IAR method should be applied.

Using our proposed WL IAR method, the estimated WL ambiguities are partially fixed, which is shown in Figure 7 for six trajectories in our experiment. Overall, the achieved fix-rates are from 57% to 70%, where a better environment can generally achieve better fix-rates. To sum up, although their observation quality is not comparable to navigational GNSS devices, WL ambiguities on smartphone devices are fixable. However, the initial conclusions suggest that a partial WL IAR strategy should

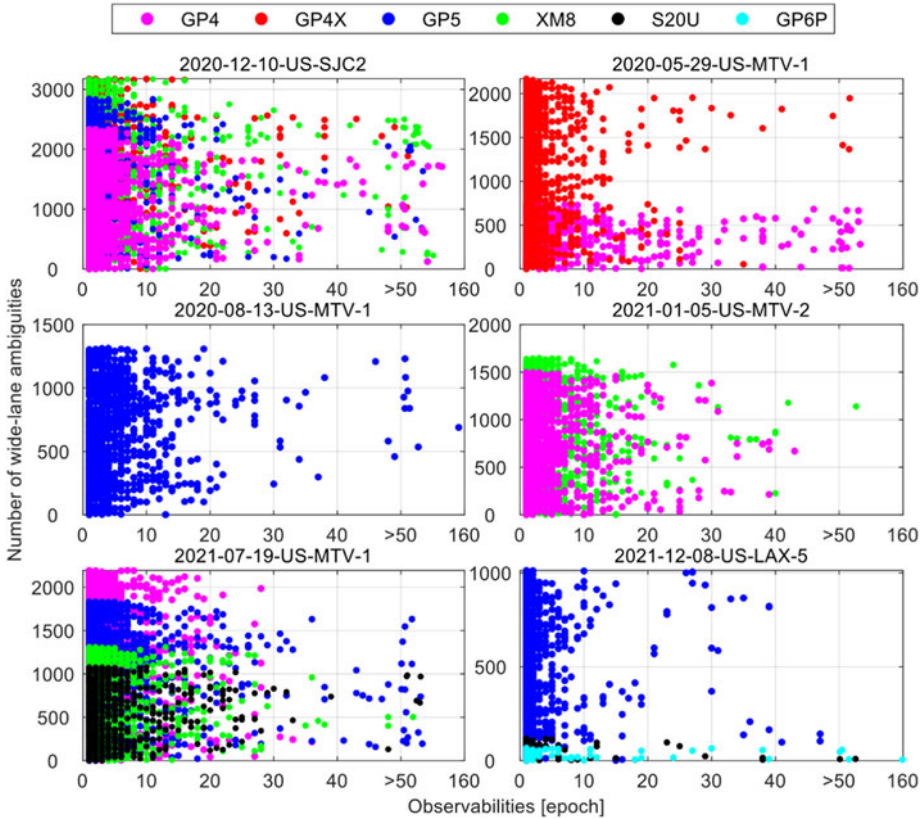


Figure 4. Numbers of WL ambiguities versus the observabilities of WL ambiguities on six trajectories with six smartphones.

be applied, due to the existence of unfixable WL ambiguities. The following section discusses the positioning performance of WL IAR, highlighting the accuracy of our proposed method.

3.2. Positioning performance with WL IAR

In this section, we evaluate the positioning performance of smartphone WL IAR by showing positioning error time series and error statistics. To compare with our proposed method, a conventional partial rounding strategy is used, which is called traditional method in the sequel. We set the rounding threshold around 0.05 cycle to partially fix the WL ambiguities. In this section, the accuracy metric of root-mean-square (RMS) is frequently used.

First, a comparison between the traditional method and the proposed method is done at some typical locations in our experiment, shown in Figure 8 with the map, where the truth and float solutions are also plotted. As demonstrated, the positioning solutions after achieving WL IAR are generally closer to the truth, while the float solution is frequently biased due to the lack of continuousness on smartphone carrier-phase measurements. After achieving WL IAR, the traditional method solution gives RMS values of 1.857 and 0.784 m in the horizontal component, which is 1.749 and 0.762 m by the proposed method. Therefore, WL IAR can benefit smartphone positioning, where the proposed method is more effective than the conventional traditional strategy.

Table 3 lists the positioning RMS values from float solutions, and traditional and proposed methods on six trajectories and six smartphones. Some data do not have the truth trajectory in the upward direction, and therefore their RMS values cannot be obtained. Overall, with WL IAR, the RMS improvements

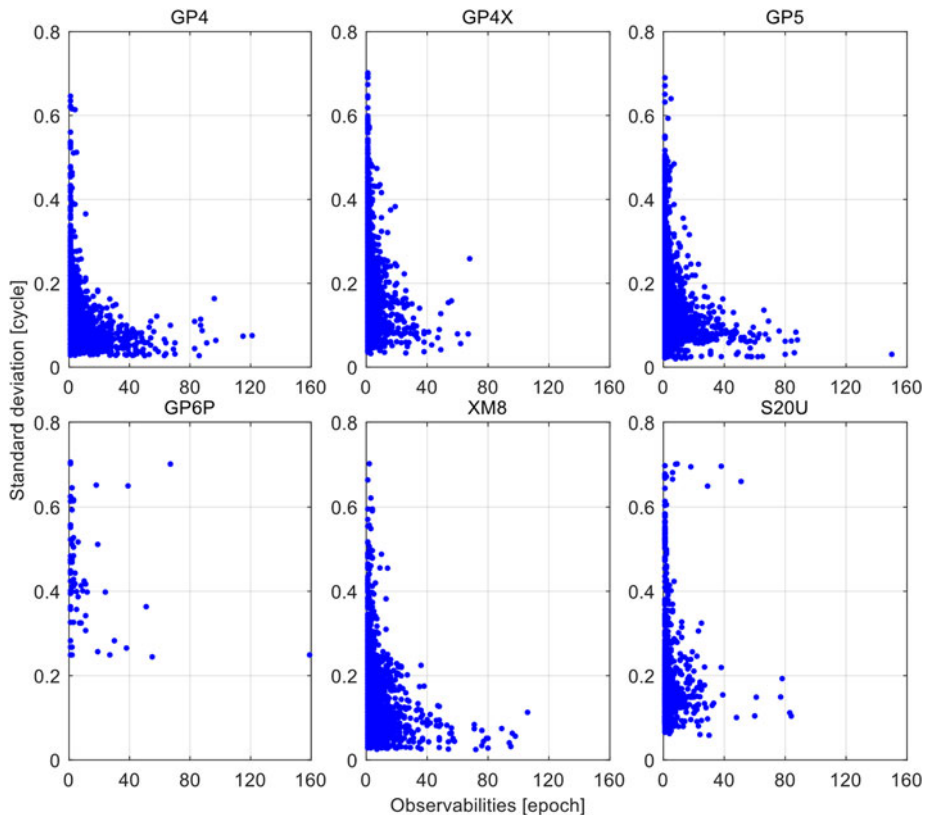


Figure 5. Variances of estimated WL ambiguities in the float solutions with respect to their observabilities on six trajectories with six smartphones.

can be witnessed on all three directions, where the traditional method improves the 3D RMS values from float solution by $2 \cdot 5\%$, and the proposed method improves by $7 \cdot 5\%$. On average, the achievable horizontal RMS values by the proposed method is $1 \cdot 687$ m, which is $1 \cdot 835$ m for the float solution and $1 \cdot 827$ m for the traditional method. For all 16 experiments, the proposed method is better than the float and traditional methods for all experiments based on 3D RMS and 14 experiments based on 2D RMS, where the traditional method is better than the proposed method only on two experiments on 2D RMS, and better than float solutions only on 57% experiments for 2D RMS and 80% for 3D RMS.

Specifically, Figure 9 provides a quantitative analysis about how much the proposed method can benefit the smartphone positioning accuracy. Here, rows 1 to 16 indicate the Tests 1 to 16, 2D RMS represents the horizontal RMS values, and 3D RMS values are missing for some datasets due to the missing of upward ground truth. On average, the proposed method can improve 2D RMS by $0 \cdot 112$ m, which is only $0 \cdot 016$ m for the traditional method. For 3D RMS, the traditional method has degraded performance on three datasets, which is 43%. Although the proposed method insignificantly degrades the 2D RMS on the last two experiments, it is improvement for 100% of all experiments when 3D RMS is considered. As a conclusion, the proposed method can improve the positioning performance by achieving smartphone partial WL IAR.

At last, Table 4 compares different smartphone models in terms of WL IAR performance. All the results of selected smartphones are depicted in. It can be seen the results with WL IAR have smaller residual values than that of float solutions. The positioning accuracy in this experiment can be improved by up to $9 \cdot 7$ cm (GP4X), and the rest are generally improved by 4–7 cm. The WL IAR fix-rate results of the smartphones are between 55% and 70% within a certain threshold.

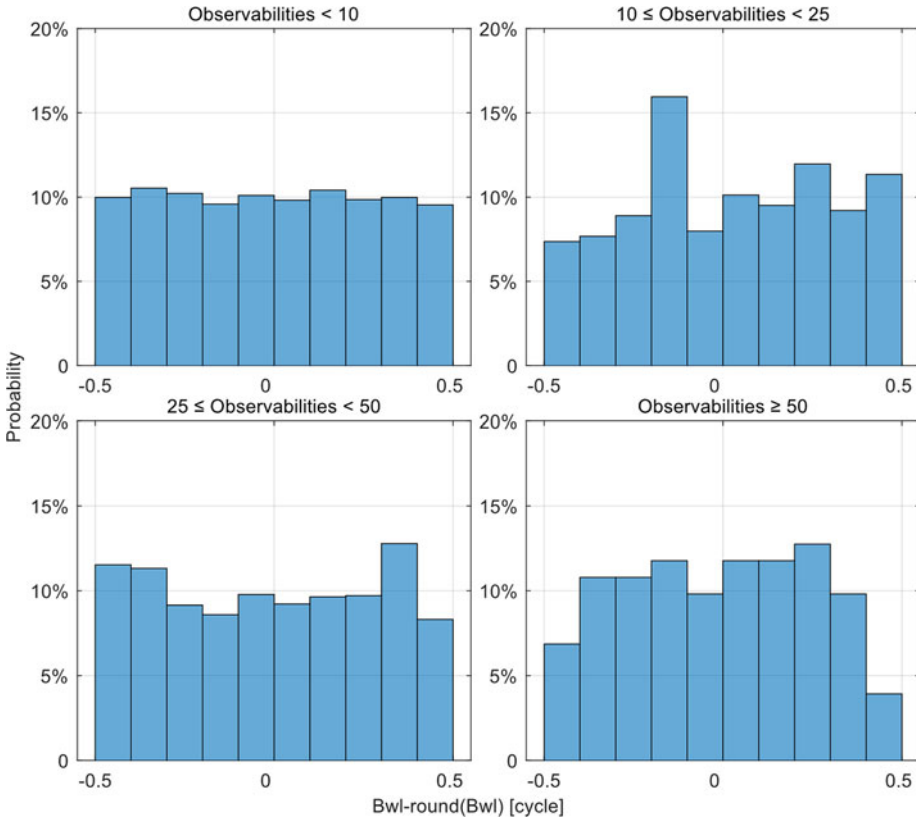


Figure 6. WL ambiguity integerness on six trajectories with six smartphones with respect to different observability levels.

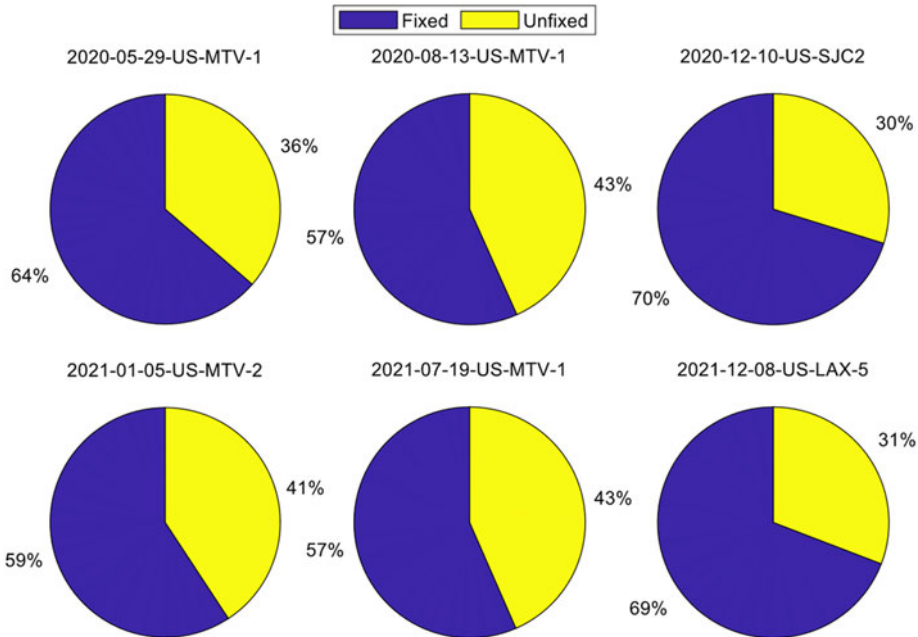


Figure 7. WL ambiguity fix-rates on six trajectories.

Table 3. Positioning RMS accuracy comparing float, traditional and proposed methods in east (E), north (N) and upward (U) directions.

Trajectory	Types	Float RMS [m]			Traditional RMS [m]			Proposed RMS [m]		
		E	N	U	E	N	U	E	N	U
2020-12-10-US-SJC-2	GP4	1.529	2.168	–	1.510	2.159	–	1.433	1.823	–
	GP4X	1.095	2.173	–	1.094	2.165	–	1.011	1.650	–
	GP5	1.168	2.043	–	1.154	1.995	–	1.166	1.877	–
	XM8	1.214	1.431	–	1.225	1.395	–	1.104	1.357	–
2020-05-29-US-MTV-1	GP4	0.642	0.752	–	0.641	0.748	–	0.611	0.725	–
	GP4X	0.598	0.755	–	0.589	0.749	–	0.482	0.703	–
2020-08-13-US-MTV-1	GP5	0.861	1.219	–	0.855	1.200	–	0.838	1.110	–
2021-01-05-US-MTV-2	GP4	0.642	0.450	–	0.651	0.448	–	0.630	0.428	–
	XM8	0.738	0.895	–	0.724	0.828	–	0.692	0.781	–
2021-07-19-US-MTV-1	GP4	0.559	1.001	1.555	0.532	0.962	1.505	0.529	0.906	1.469
	GP5	0.471	0.720	0.828	0.485	0.687	0.856	0.400	0.694	0.768
	XM8	0.817	1.574	2.923	0.816	1.564	3.157	0.811	1.517	2.780
2021-12-08-US-LAX-5	S20U	0.564	1.334	1.928	0.581	1.347	1.900	0.525	1.327	1.799
	GP5	0.874	0.794	1.949	0.867	0.776	1.920	0.745	0.789	1.858
	GP6P	0.700	0.606	1.480	0.702	0.609	1.386	0.670	0.672	1.223
	S20U	0.919	0.846	1.126	0.920	0.845	1.165	0.864	0.915	0.981



Figure 8. Typical positioning performances on the map of the truth, float, traditional and proposed method solutions of straight and bend conditions.

4. Conclusions

In this study, we propose a method to achieve partial WL IAR for smartphones which considers the existence of ambiguity biases to minimize their effect. In the first step, the float ambiguities that are with significant confidence function values are processed with integer rounding. In the second step, the remaining float ambiguities are handled by the LAMBDA method. Based on a dataset from GSDC 2022, the performance of the proposed method is evaluated in terms of aspects of positioning accuracy and WL ambiguity quality for different models of smartphones. A few conclusions can be made:

1. Due to poor observability, the WL ambiguities on smartphone devices are only partially fixable. In our experiment, the achieved fix-rates are from 57% to 70%.
2. The proposed WL IAR method in this study can achieve effective WL IAR solutions, which on average improve the positioning accuracy by $7 \cdot 7\%$ for the horizontal components. But the conventional WL IAR method can only improve by $1 \cdot 1\%$.
3. In terms of smartphone models, similar and comparable performances of WL IAR can be achieved from GP4, GP4X, GP5, GP6P, XM8, S20, as detailed in [Table 4](#).

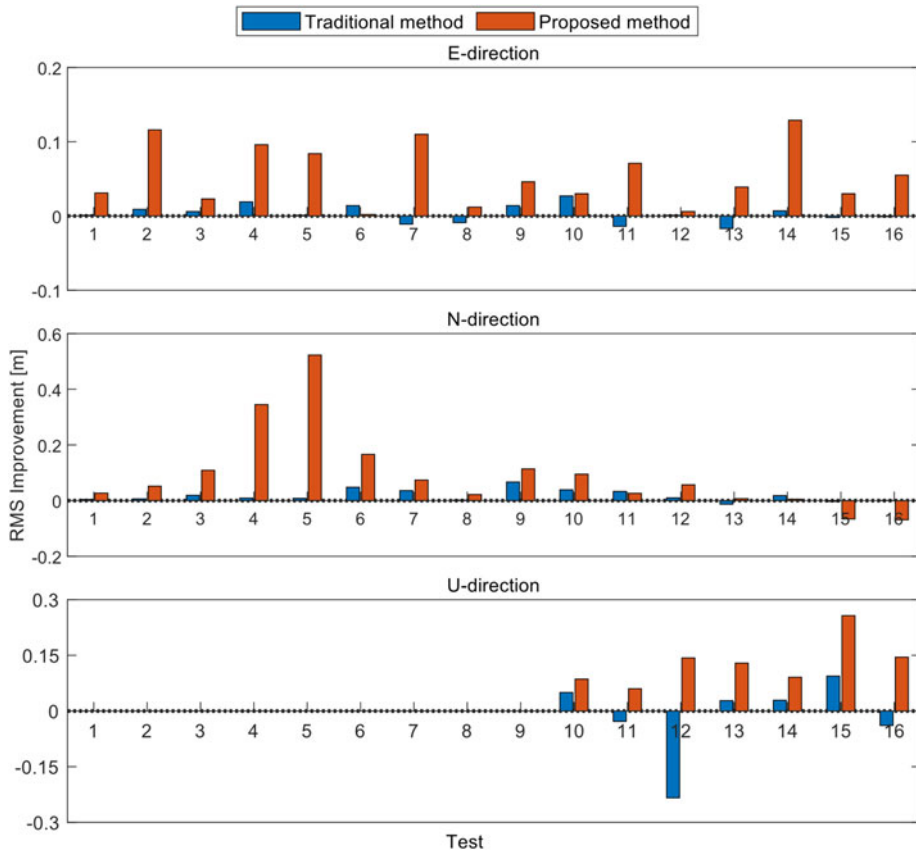


Figure 9. WL IAR accuracy improvements from float to traditional and proposed methods. The order of number of experiments are aligned with Table 3.

Table 4. Comparison of six smartphone models in terms of WL ambiguity resolution performance.

Phone types	Float accuracy [m]	WL IAR accuracy [m]	WL IAR fix-rate	WL noise [cycle]
GP4	0.900	0.851	61.3%	0.114
GP4X	0.847	0.750	68.7%	0.193
GP5	0.852	0.814	64.9%	0.145
GP6P	0.700	0.670	57.4%	0.441
XM8	0.943	0.888	70.3%	0.145
S20	0.700	0.655	54.7%	0.202

Future work should include the real-time WL IAR implementation and narrow-lane ambiguity resolution in smartphone kinematic positioning, which may be an impressive work in real application. Continuously fixed WL ambiguity resolution will provide reliability and accuracy to smartphone real-time narrow-lane ambiguity resolved solutions. Therefore, as a future study, smartphone narrow-lane ambiguity resolution can be implemented to complete the accuracy promotion for smartphone applications.

References

- Brommer, C., Jung, R., Steinbrener, J. and Weiss, S.** (2020). MaRS: A modular and robust sensor-fusion framework. *IEEE Robotics and Automation Letters*, **6**(2), 359–366. doi:10.1109/LRA.2020.3043195
- Castel, B., Cortés, I., Merwe, J., Dietmayer, K., Rugamer, A. and Felber, W.** (2021). Evaluation of Decimeter Positioning Post-Processing Algorithms Using GNSS Raw Measurements. *Proc. ION GNSS+ 2021*, Institute of Navigation, St. Louis, Missouri, September 20–24, pp. 3037–3048. doi:10.33012/2021.18051
- Dabove, P. and Di Pietra, V.** (2019a). Single-baseline RTK positioning using dual-frequency GNSS receivers inside smartphones. *Sensors*, **19**(19), 4302. doi:10.3390/s19194302
- Dabove, P. and Di Pietra, V.** (2019b). Towards high accuracy GNSS real-time positioning with smartphones. *Advances in Space Research*, **63**(1), 94–102. doi:10.1016/j.asr.2018.08.025
- Dai, S.** (2022). 2nd Place Winner of the Smartphone Decimeter Challenge: Improving Smartphone GNSS Positioning Using Gradient Descent Method. *Proc. ION GNSS+ 2022*, Denver, Colorado, USA, September 19–23, pp. 2321–2328. doi:10.33012/2022.18380
- Dong, D. N. and Bock, Y.** (1989). Global positioning system network analysis with phase ambiguity resolution applied to crustal deformation studies in California. *Journal of Geophysical Research: Solid Earth*, **94**(B4), 3949–3966. doi:10.1029/JB094iB04p03949
- Dong, X., Zhang, L., Lv, R. and Cai, Y.** (2022). An Adaptive Nonlinear Filter for Uncertain Measurement Noise. In *Advances in Guidance, Navigation and Control: Proceedings of 2020 International Conference on Guidance, Navigation and Control, ICGNC 2020*, Tianjin, China, October 23–25, pp. 4089–4100. Springer Singapore. doi:10.1007/978-981-15-8155-7_341
- Engelbrecht, J., Booyens, M. J., van Rooyen, G. J. and Bruwer, F. J.** (2015). Survey of smartphone-based sensing in vehicles for intelligent transportation system applications. *IET Intelligent Transport Systems*, **9**(10), 924–935. doi:10.1049/iet-its.2014.0248
- Fortunato, M., Tagliaferro, G., Fernández-Rodríguez, E. and Critchley-Marrows, J.** (2021). The Whole Works: A GNSS/IMU Tightly Coupled Filter for Android Raw GNSS Measurements with Local Ground Augmentation Strategies. *Proc. ION GNSS+ 2021*, Institute of Navigation, St. Louis, Missouri, USA, September 20–24, pp. 3103–3126. doi:10.33012/2021.18006
- Fu, G. M., Khider, M. and Van Diggelen, F.** (2020). Android Raw GNSS Measurement Datasets for Precise Positioning. *Proc. ION GNSS+ 2020*, Institute of Navigation, September 21–25, pp. 1925–1937. doi:10.33012/2020.17628
- Fu, G. M., Khider, M. and Van Diggelen, F.** (2022). Summary and Legacy of the Smartphone Decimeter Challenge (SDC) 2022. *Proc. ION GNSS+ 2022*, Institute of Navigation, Denver, Colorado, USA, September 19–23, pp. 2301–2320. doi:10.33012/2022.18379
- Gao, R., Xu, L., Zhang, B. and Liu, T.** (2021). Raw GNSS observations from android smartphones: Characteristics and short-baseline RTK positioning performance. *Measurement Science and Technology*, **32**(8), 084012. doi:10.1088/1361-6501/abe566
- Gao, Y., Zangenehnej, F., Jiang, Y. and Zhang, Y.** (2023). Fast High Accuracy Kinematic Smartphone Positioning for Location-Based Services. Abstracts of the ICA, **6**, 67. doi:10.5194/ica-abs-6-67-2023
- Ge, M., Gendt, G., Rothacher, M. A., Shi, C. and Liu, J.** (2008). Resolution of GPS carrier-phase ambiguities in precise point positioning (PPP) with daily observations. *Journal of Geodesy*, **82**(7), 389. doi:10.1007/s00190-007-0187-4
- Geng, J. and Bock, Y.** (2013). Triple-frequency GPS precise point positioning with rapid ambiguity resolution. *Journal of Geodesy*, **87**(5), 449–460. doi:10.1007/s00190-013-0619-2
- Geng, J. and Li, G.** (2019). On the feasibility of resolving android GNSS carrier-phase ambiguities. *J Geod*, **93**, 2621–2635. doi:10.1007/s00190-019-01323-0
- Geng, J., Teferle, F. N., Meng, X. and Dodson, A. H.** (2011). Towards PPP-RTK: Ambiguity resolution in real-time precise point positioning. *Advances in Space Research*, **47**(10), 1664–1673. doi:10.1016/j.asr.2010.03.030
- GSA** (2018a). World's First Dual-Frequency GNSS Smartphone Hits the Market. GSA. Available at <https://www.euspa.europa.eu/newsroom/news/world-s-first-dual-frequency-gnss-smartphone-hits-market>
- GSA** (2018b). Using GNSS Raw Measurements on Android Devices. Available at <https://www.gsa.europa.eu/newsroom/news/available-now-white-paper-using-gnss-raw-measurements-android-devices>.
- Gu, S., Lou, Y., Shi, C. and Liu, J.** (2015). Beidou phase bias estimation and its application in precise point positioning with triple-frequency observable. *Journal of Geodesy*, **89**(10), 979–992. doi:10.1007/s00190-015-0827-z
- Han, K., Lee, S., Song, Y. J., Lee, H. B., Park, D. H. and Won, J. H.** (2021). Precise Positioning with Machine Learning Based Kalman Filter Using GNSS/IMU Measurements From Android Smartphone. *Proc. ION GNSS+ 2021*, Institute of Navigation, St. Louis, Missouri, USA, September 20–24, pp. 3094–3102. doi:10.33012/2021.18005
- Hatch, R.** (1983). The Synergism of GPS Code and Carrier Measurements. In *International Geodetic Symposium on Satellite Doppler Positioning*, Vol. 2, pp. 1213–1231.
- Hu, J., Li, P. and Bisnath, S.** (2023). Towards GNSS Ambiguity Resolution for Smartphones in Realistic Environments: Characterization of Smartphone Ambiguities with RTK, PPP, and PPP-RTK. In *Proceedings of the 36th International Technical Meeting of the Satellite Division of The Institute of Navigation (ION GNSS+ 2023)*, pp. 2698–2711. doi:10.33012/2023.19285
- Jiang, Y., Gao, Y., Ding, W. and Gao, Y.** (2022). GNSS precise positioning for smartphones based on the integration of factor graph optimization and solution separation. *Measurement*, **203**, 111924. doi:10.1016/j.measurement.2022.111924
- Kanhere, A. V., Gupta, S., Shetty, A. and Gao, G.** (2021). Improving GNSS Positioning Using Neural Network-Based Corrections. *Proc. ION GNSS+ 2021*, Institute of Navigation, St. Louis, Missouri, USA, September 20–24, pp. 3068–3080. doi:10.33012/2021.17999

- Li, G. and Geng, J.** (2022). Android multi-GNSS ambiguity resolution in the case of receiver channel-dependent phase biases. *Journal of Geodesy*, **96**(10), 1–18. doi:10.1007/s00190-022-01656-3
- Li, Y., Cai, C. and Xu, Z.** (2022a). A combined elevation angle and C/N0 weighting method for GNSS PPP on Xiaomi MI8 smartphones. *Sensors*, **22**(7), 2804. doi:10.3390/s22072804
- Li, B., Miao, W., Chen, G. E. and Li, Z.** (2022b). Ambiguity resolution for smartphone GNSS precise positioning: Effect factors and performance. *Journal of Geodesy*, **96**(9), 1–18. doi:10.1007/s00190-022-01652-7
- Melbourne, W. G.** (1985). The Case for Ranging in GPS-Based Geodetic Systems. In: *Proceedings of 1st International Symposium on Precise Positioning with the Global Positioning System*, Rockville, MD, pp. 373–386.
- Paziewski, J.** (2020). Recent advances and perspectives for positioning and applications with smartphone GNSS observations. *Measurement Science and Technology*, **31**(9), 091001. doi:10.1088/1361-6501/ab8a7d
- Realini, E., Caldera, S., Pertusini, L. and Sampietro, D.** (2017). Precise GNSS positioning using smart devices. *Sensors*, **17**(10), 2434. doi:10.3390/s17102434
- Song, H., Cheng, S., Xu, Z. and Zang, N.** (2022). Research on PPP/INS Algorithm Based on Sequential Sage-Husa Adaptive Filtering. In *China Satellite Navigation Conference (CSNC 2022) Proceedings: Volume I*, pp. 374–383. Singapore: Springer Nature Singapore. doi:10.1007/978-981-19-2588-7_35
- Suzuki, T.** (2021). First Place Award Winner of the Smartphone Decimeter Challenge: Global Optimization of Position and Velocity by Factor Graph Optimization. *Proc. ION GNSS+ 2021*, Institute of Navigation, St. Louis, Missouri, USA, September 20–24, pp. 2974–2985. doi:10.33012/2021.18109
- Suzuki, T.** (2022). Two-Step Optimization of Velocity and Position Using Smartphone's Carrier Phase Observations. *Proc. ION GNSS+ 2022*, Institute of Navigation, Denver, Colorado, USA, September 19–23, pp. 276–2286. doi:10.33012/2022.18377
- Teunissen, P. J.** (1993). Least-Squares Estimation of the Integer GPS Ambiguities. In *Invited Lecture, Section IV Theory and Methodology, IAG General Meeting*, Beijing, China, pp. 1–16
- Teunissen, P. J.** (2001). Statistical GNSS Carrier Phase Ambiguity Resolution: A Review. In *Proceedings of the 11th IEEE Signal Processing Workshop on Statistical Signal Processing (Cat. No. 01TH8563)*, pp. 4–12. IEEE. doi:10.1109/SSP.2001.955208
- Wen, Q., Geng, J., Li, G. and Guo, J.** (2020). Precise point positioning with ambiguity resolution using an external survey-grade antenna enhanced dual-frequency android GNSS data. *Measurement*, **157**, 107634. doi:10.1016/j.measurement.2020.107634
- Wübbena, G.** (1985). Software Developments for Geodetic Positioning with GPS Using TI-4100 Code and Carrier Measurements. In: *Proceedings of 1st International Symposium on Precise Positioning with the Global Positioning System*, Rockville, MD, pp 403–412.
- Yong, C. Z., Harima, K., Rubinov, E., McClusky, S. and Odolinski, R.** (2022). Instantaneous best Integer equivariant position estimation using google pixel 4 smartphones for single-and dual-frequency, multi-GNSS short-baseline RTK. *Sensors*, **22**(10), 3772. doi:10.3390/s22103772
- Zeng, S., Kuang, C. and Yu, W.** (2022). Evaluation of real-time kinematic positioning and deformation monitoring using Xiaomi Mi 8 smartphone. *Applied Sciences*, **12**, 435. doi:10.3390/app12010435